MedCrave
Step into the World of Research
Aeronautics and Aerospace Open access Journal

Research Article

Open Access

CrossMark

Compact gravity wave detector

Abstract

An incoming gravity wave being a stress wave is a surface with intrinsic curvature. When a light beam is parallel transported on this non-Euclidian surface it acquires an excess phase which accumulates with each circuit. We calculate the separate contributions to excess phase from the wave geometry as well as the dynamic response of mirrors in a Michelson interferometer. Using these results and a combination of analogue and digital signal processing techniques we show how a compact interferometer can be made sensitive to gravity waves of amplitude density $10^{-23}/\sqrt{\text{Hz}}$ within a frequency range 10^{-4}Hz to 10^{4}Hz. As an example we describe a 10cm Michelson interferometer designed to measure gravity waves from sources as far as the Virgo cluster.

Keywords: principle of equivalence, spacetime geometry, sampled detection, gravity waves

Volume 10 Issue 3 - 2026

Munawar Karim,[1] Kris Green[2]

[1]Department of Biology, Chemistry and Physics, Namibia University of Science and Technology, Windhoek, NAMIBIA

[2]Department of Mathematics and Computer Science, St. John Fisher University, Rochester, NY 14618, USA

Correspondence: Munawar Karim, Department of Biology, Chemistry and Physics, Faculty of Natural and Applied Sciences, Namibia University of Science and Technology, Windhoek, Namibia, Email mkarim@icloud.com

Received: August 14, 2026 | **Published:** August 31, 2026

Introduction

Following earlier attempts by Weber.,[1] Forward.,[2,3] and Weiss,[4] several groups have been engaged in building detectors and observatories to study gravitational radiation from astrophysical sources. Among those which seem most likely to emit signals strong enough and often enough to trigger current detectors are inspiralling binary neutron stars from distances up to the Virgo cluster.

Gravitational waves have been detected in 2016.[5]

Detectors may be classified as either resonant mass or interferometric. We will be concerned with the latter only. Interferometric detectors rely on detecting relative phase changes between a pair of mutually orthogonal light beams intersecting a pulse of gravitational radiation.

Interference patterns jiggle because of momentary differences in the time-delay caused by metric perturbations due to a pulse of a passing gravity wave.

Sensitivity calculations

Interference patterns can also be disturbed by noise from Brownian motion and radiation pressure. The gravity wave signal, to be detectable, has to overcome these noise sources. The sensitivity is calculated by comparing contributions to the time jitter from all sources. This method gives a direct result because it relates to the time delay - the quantity being measured.

The interferometer arms are aligned along the $x-$ and $y-$ axes. The arms are of length L as measured in flat space. The gravitational wave described by a four-vector $k_o = (\omega, k)$, which is incident along the $z-$ axis, perturbs the metric by a small amplitude. The back ground is a flat metric ($\eta_{\mu\nu}$); the perturbed metric is:

$$g_{\mu\upsilon} = \eta_{\mu\nu} + h_{\mu\nu} \tag{1}$$

A null vector represents light in the interferometer. Because of the $x-$ and $y-$alignment of the arms we need consider only the (1,1) and (2,2) components of the metric: the beam splitter is in free fall. The mirrors may or may not be in free fall, we will treat the general case.

$$ds^2 = 0 = g_{\mu\upsilon} dx^{\mu} dx^{\nu} = (\eta^{\mu\nu} + h^{\mu\nu})\, dx^{\mu} dx^{\nu} \tag{2}$$

$$0 = -c^2 dt^2 + [1 + \mathrm{h}_{11}(\omega t - \mathrm{k}\cdot\mathrm{x})]\, dx^2 \tag{3}$$

The gravity wave affects both time and space components. The gravity wave does not change the coordinate length L, which is altered to proper length $L_x = L + \xi^1$. Christodoulou has shown that the wave is a stress wave and thus has a non-linear memory,[5] this property, as well as the measure of proper time, requires the use of proper length. Along the $x-$ axis the round-trip light travel time is:

$$\tau_{rt} = \frac{2L_x}{c} + \frac{1}{2c}\int_0^{Lx} \mathrm{h}_{11}(\omega t - \mathrm{k.x})dx - \frac{1}{2c}\int_{Lx}^{0} \mathrm{h}_{11}(\omega t - \mathrm{k.x})dx \tag{4}$$

A similar integral appears for the $y-$ axis with h_{22} substituted for h_{11} and the limit $\mathrm{L}_y = \mathrm{L} + \xi^2$. In the transverse traceless gauge we are working with $\mathrm{h} = \mathrm{h}_{11} = -\mathrm{h}_{22}$; the arm lengths are affected in opposite directions. h is assumed to be constant over the range of the integral.

The integrals may be evaluated to obtain the difference in round-trip travel times between the $x-$ and $y-$axes. The time difference is:

$$\Delta\tau_i = 2\frac{\xi_i^1 - \xi_i^2}{c} + h(t)\frac{2L_i}{c} = \frac{\xi_i^1 - \xi_i^2}{L}\tau_i + h(t)\tau_i \tag{5}$$

where τ_i is the proper round-trip time for the i-th beam traversing the interferometer:

$$\Delta\tau_i = \left[\frac{L_x + L_y}{c}\right] = \frac{2L_i}{c} \tag{6}$$

obtained after setting $\xi_i^1 = -\xi_i^2$. A general reference for this discussion is Saulson.[5]

In the interferometer we are describing, independent light beams traverse the interferometer several times. Each round-trip on the wave front, since it is a curved surface, accrues a time delay of $\Delta\tau_i$. Again because of intrinsic curvature the time delay accumulates with each circuit. For p round-trips the total time delay is $p\Delta\tau_i$ (for a constant h, since $\Delta\tau_i \ll$ duration of the gravity wave pulse, this is a reasonable assumption). Each circuit or sample is τ_i in duration. This method of sampling requires identification of the i-th beam. The interference intensity is recorded in discrete samples.

The metric of the incident gravity wave has intrinsic curvature (non-zero Riemann tensor), implying a wave-front surface that is saddle-like (Figure 1) (see[6]). The time delay $\Delta\tau_i$ may be interpreted

Submit Manuscript | http://medcraveonline.com

©2026 Karim et al. This is an open access article distributed under the terms of the Creative Commons Attribution License, which permits unrestricted use, distribution, and build upon your work non-commercially.

Copyright: ©2026 Karim et al.

as the excess angle $\Delta\varphi_i$ acquired by a null-vector (light beam) parallel transported simultaneously along two closed loops ($x-$ and $y-$axes), on a surface with intrinsic curvature.

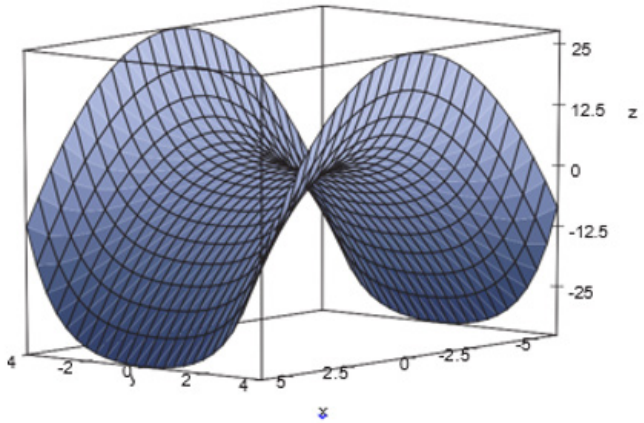

Figure 1 Surface of gravity wave-front. Shown is the field amplitude hμν along the z - axis: at this instant h_{11} is negative and h_{22} is positive. The surface has intrinsic curvature. An excess phase appears in a null vector parallel transported in a circuit on this surface. $\Delta\varphi_i$ is the difference in excess phase between a circuit along the *x* — and *y* — axes.

Response of interferometer and mirror mount

The interferometer responds to the incident gravity wave. The interferometer is a rigid platform. It is accelerating upwards to counter Earth's gravity. It is in principle not in an inertial frame. Acceleration, in principle, affects both mirror spacing and time delay. These effects are taken care of by equations of special relativity. For a detailed discussion and experimental confirmation see.[7–10] For a system accelerating @g ≈ 10m/sec$_2$, times and lengths will change according to:[11]

$$t = t_0 + (c/g)\sinh(g\tau/c) \quad \text{and} \quad x = x_o + (c^2/g)[\cosh(g\tau/c) - 1]$$

For measurement intervals $\tau \ll 1$secs there is negligible change in either *t* or *x*. Acceleration is not an issue, the platform is in practice, inertial.

What is the effect of the rigid platform? The time delay Eq.(5) is the sum of contributions from time and space components.

Since the phase of a plane wave is an invariant quantity i.e., $\varphi = \omega t - k\cdot x = \omega' t' - k'\cdot x'$, a change in phase in general stems from a change in both time and space components. The gravity wave has two independent effects; (i) it alters clock rates (ii) it affects lengths. Just as the gravity wave changes the time delay from $\tau_i \rightarrow \tau_i + h\tau_i$, so does it alter the length $2L \rightarrow 2L+h2L$. A quick way to see why there are two independent sources of the phase is to follow the world lines of the light rays emerging from the beam-splitter as they reflect off the two mirrors (Figure 2). The mirrors are shown in two configurations: (i) in free fall and (ii) attached rigidly to the interferometer. In the freely falling frame of the beam-splitter the limits of the integrals in Eq.(4) are changed from 0 to L to 0 to L + ξ^1 and 0 to L +ξ^2 along the $x-$ and $y-$ axes respectively. The mirrors appear displaced in the same sense (as they must be for the ratio to be c, the speed of light measured by local observers) as in the freely falling case, but less so in the case of rigid mounts. In either case, whether in free fall or rigidly attached, there is still a phase difference because of the intrinsic curvature in the wave-front surface. Time and space components are affected independently. A quantitative discussion follows.

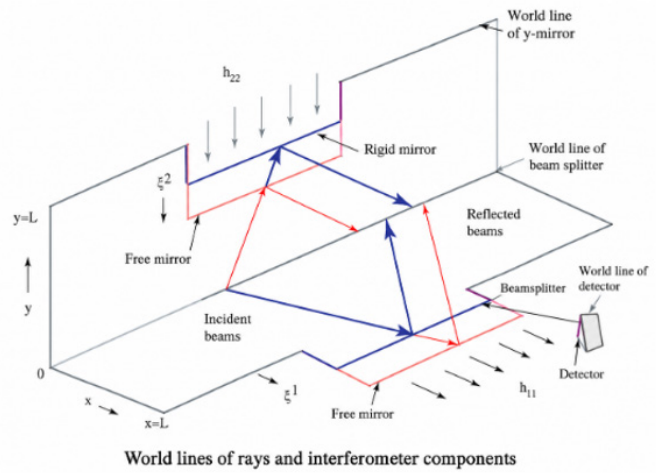

Figure 2 World lines of rays and interferometer components. Two mirror mounts, free in light and rigid in heavy lines, are shown under the influence of a gravity wave of constant amplitude $h_{\mu\nu}$. Although the surfaces are shown as planes they are saddle-shaped as in figure 1. The reflection points depend on the type of mirror mount, and so does the excess phase.

In our calculation the beam-splitter and mirrors may be treated as test masses in free fall, or the mirrors may be attached rigidly to the interferometer platform. In the former case the mirrors and beam-splitter move along individual geodesics.

Whene h_{jk} is time-varying as is the case for gravity waves, one can calculate the response as follows: For the general case consider the mirrors as test masses connected through a spring of coordinate length *L*, force constant k^μ_α with damping constant b^μ_α . The interferometer is in free fall. We may use geodesic coordinates where the Christoffel symbols are made zero[12] on all points on the geodesic. The geodesic is the world line of the beam-splitter. The time coordinate is along the instantaneous tangent to the world line of the beam-splitter. There is an orthogonal co-moving coordinate with the mirror lying on the $x-$axis. The quantities ($h^\mu_\alpha = h$, $k^\mu_\alpha = k$, $b^\mu_\alpha = b$) have only one component. The equation of motion which describes the mirror of mass m that has an instantaneous position x^1 is[1] with appropriate modifications:

$$\frac{\partial^2 x^1}{\partial t^2} + \frac{b}{m}\frac{\partial x^1}{dt} + \omega_0^2(x^1 - L) = -R^{GW}_{1010}x^1 = \frac{1}{2}\frac{\partial^2 h_{11}}{\partial t^2}x^1 = -\frac{1}{2}\omega^2 x^1 h_{11} \qquad (7)$$

$$\frac{\partial^2 x^1}{\partial t^2} + \frac{b}{m}\frac{\partial x^1}{dt} + (\omega_0^2 + \frac{1}{2}\omega^2 h_{11}\sin\omega t)x^1 = \omega_0^2 L$$

where $h_{jk} = h_{jk}\, sin\ \omega t$ and the fundamental mode is $\omega_0^2 \equiv$ k/m; *L* is the relaxed length of the spring. This is an inhomogeneous form of Hill's equation (for $b = 0$). What we observe here is that, under the action of the gravity wave, the mirror oscillates with a frequency that varies sinusoidally with a frequency-dependent amplitude of O(*h*).

Eq.(7) says that the elastic properties of the mirror suspension, whether "soft" or rigid, depending as they do on the speed of sound in the platform, and therefore on lengths and time, are modulated by the incident gravity wave.

We re-write this equation for $(b/m) \ll 1$ or $Q \equiv \omega_0 m/b \gg 1$.

$$\frac{\partial^2 x^1}{\partial t^2} + (\omega_0^2 + \frac{1}{2}\omega^2 h_{11}\sin\omega t)x^1 = \omega_0^2 L \qquad (8)$$

This equation may be simplified by defining a new dynamic variable $\epsilon^1 \equiv (x^1 - L)/L = \xi^1/L$. In terms of this new variable Eq. (8) becomes

Copyright: ©2026 Karim et al.

$$\frac{\partial^2 \epsilon^1}{\partial t^2} + (\omega_0^2 + \frac{1}{2}\omega^2 h_{11} \sin\omega t)\,\epsilon^1 = \frac{1}{2}\omega^2 h_{11} \sin\omega t \quad (9)$$

This equation describes, with appropriate choice of ω_0, any type of mirror suspension, whether soft or stiff. We use an iterative process to solve this equation. Using a small 4 expansion parameter $q = 1/2\ h_{11}(\omega/\omega_0)^2 \equiv 1/2\ ha^2$ (recall that $h_{11} \ll 1$),we assume a series solution of the form

$$\epsilon^1(t) = \sum_{n=0}^{\infty} q^n \epsilon_n^1(t) \quad (10)$$

With initial conditions $\epsilon^1\Big|_{t=0} = \frac{\partial \epsilon^1}{\partial t}\Big|_{t=0} = 0$ to O(h), ,the solution of Eq. (9) is

$$\epsilon^1 \approx \frac{1}{2} h_{11} \frac{\omega^2}{(\omega_0^2 - \omega^2)}\left(\frac{\omega}{\omega_0}\sin\omega_0 t - \sin\omega t\right);\ \omega \neq \omega_0 \quad (11)$$

For the mirror on the y – axis there is a similar equation:

$$\frac{\partial^2 \epsilon^2}{\partial t^2} + (\omega_0^2 + \frac{1}{2}\omega^2 h_{22} \sin\omega t)\,\epsilon^1 = -\frac{1}{2}\omega^2 h_{22} \sin\omega t \quad (12)$$

with a similar solution:

$$\epsilon^2 \approx \frac{1}{2} h_{22} \frac{\omega^2}{(\omega_0^2 - \omega^2)}\left(\frac{\omega}{\omega_0}\sin\omega_0 t - \sin\omega t\right);\ \omega \neq \omega_0$$

The difference is, with $h = h_{11} = -h_{22}$:

$$\epsilon^1 - \epsilon^2 = \frac{\xi_i^1 - \xi_i^2}{L} = h\frac{\omega^2}{(\omega_0^2 - \omega^2)}\left(\frac{\omega}{\omega_0}\sin\omega_0 t - \sin\omega t\right);\ \omega \neq \omega_0 \quad (13)$$

This is a general solution which gives the time evolution of the strain for mirrors mounted on a platform with arbitrary stiffness characterized by resonant frequency $\omega_0/2\pi$. The free mass case is obtained by setting $\omega_0 = 0$ in Eq. (9); the solution for which is $\epsilon^1\ \epsilon^2 = h\ (\sin\omega t - \omega t)$. The steady drift is evident (Figure 3), (different from that in ref[12]). A graph of the right hand side of Eq. (13) is illustrative. For two extremes of mirror suspension, soft and stiff, one can plot the time response of the mirrors. These are shown in Figure 3 and Figure 4. The soft suspension emulates a free mass. The (almost) free mirrors drift away from their equilibrium position with each passing cycle of the gravity wave, confirming the memory effect predicted by Christodoulou.[5] By contrast the stiff mirror undergoes miniscule periodic excursions about its equilibrium position.

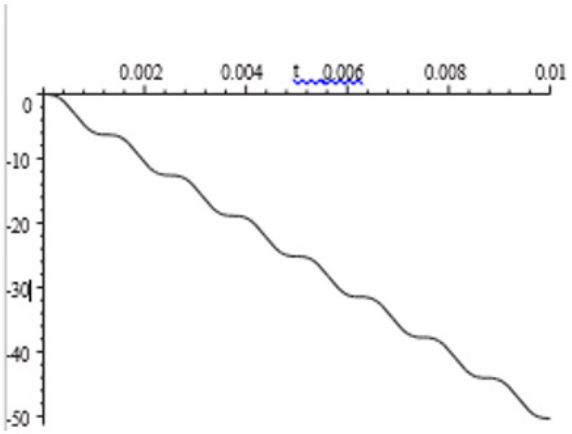

Figure 3 Mirror response in units of gravitational wave amplitude h to incoming gravity wave of maximum frequency $\omega = 2\pi \times 800s^{-1}$ and duration 10*ms*. Suspension frequency is set at 1*Hz*.

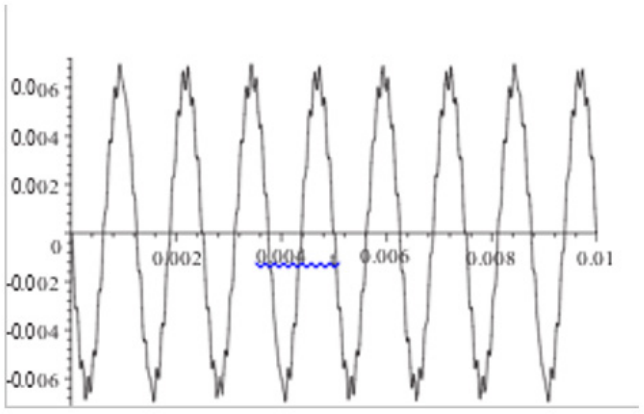

Figure 4 Mirror response in units of h to incoming gravity wave of maximum frequency $\omega = 2\pi \times 800s^{-1}$ and duration 10*ms*. Suspension frequency is set at 10^4*Hz*.

We re-write Eq. (13) as the excess proper time for the i-th sample:

$$\frac{\xi_i^1 - \xi_i^2}{L} = h\frac{\omega^2}{(\omega_0^2 - \omega^2)}\left(\frac{\omega}{\omega_0}\sin\omega_0 \tau_i - \sin\omega\tau_i\right);\ \omega \neq \omega_0 \quad (14)$$

Substitution into Eq.(5) gives

$$\Delta\tau_i = \tau_i h + \tau_i h\frac{\omega^2}{(\omega_0^2 - \omega^2)}\left(\frac{\omega}{\omega_0}\sin\omega_0 \tau_i - \sin\omega\tau_i\right);\ \omega \neq \omega_0 \quad (15)$$

For each traverse. For p independent samples the total excess time is (recall the non-Euclidian geometry of the wave surface):

$$\sum_{i=1}^{p}\Delta\tau_i = p\Delta\tau_i = p\tau_i h + h\frac{\omega^2}{(\omega_0^2 - \omega^2)}\sum_{i=1}^{p}\tau_i\left(\frac{\omega}{\omega_0}\sin\omega_0 \tau_i - \sin\omega\tau_i\right);\ \omega \neq \omega_0 \quad (16)$$

Time and space contributions add in phase because the speed of sound in the platform material, sapphire is $\approx 10^4 m/$ sec; the mirrors respond almost instantaneously i.e., within $0.10m/10^4 m/s = 10\mu$ sec, much less than the period 1/800 sec. The time delay can be related to the phase difference in monochromatic light beams of wavelength λ:

$$\Delta\phi_i = \Delta\tau_i \frac{2\pi c}{\lambda} \quad (17)$$

The total phase difference is the sum of the time and space contributions. Substituting into Eqs. (5,17)

$$\Delta\phi_i = \tau_i h\frac{2\pi c}{\lambda} + 2\frac{\xi_i^1 - \xi_i^2}{c}\frac{2\pi c}{\lambda} = \tau_i h\frac{2\pi c}{\lambda} + \tau_i h\frac{2\pi c}{\lambda}\frac{\omega^2}{(\omega_0^2 - \omega^2)}\left(\frac{\omega}{\omega_0}\sin\omega_0 \tau_i - \sin\omega\tau_i\right);$$

$$\omega \neq \omega_0 \quad (18)$$

This is the phase-shift for each pass through the interferometer. For p independent passes the accumulated phase is

$$\Delta\phi = \sum_{i=1}^{p}\Delta\phi_i = p\Delta\phi_i = p\tau_i h\frac{2\pi c}{\lambda} + h\frac{2\pi c}{\lambda}\left[\frac{\omega^2}{(\omega_0^2 - \omega^2)}\sum_{i=1}^{p}\tau_i\left(\frac{\omega}{\omega_0}\sin\omega_0 \tau_i - \sin\omega\tau_i\right)\right] \quad (19)$$

We can evaluate the second term by writing the sum as an integral with limits $t = 0$ to $t = 0.01$ sec s. Thus

$$\frac{\omega^2}{(\omega_0^2-\omega^2)}\sum_{i=1}^{p}\tau_i\left(\frac{\omega}{\omega_0}\sin\omega_0\tau_i-\sin\omega\tau_i\right)\rightarrow\frac{(\omega/\omega_0)^2}{1-(\omega/\omega_0)}\int_0^{0.01}d\tau\left(\frac{\omega}{\omega_0}\sin\omega_0\tau-\sin\omega\tau\right) \tag{20}$$

For a soft suspension $\omega_0 = 2\pi$, we choose a maximum driving frequency of $\omega = 2\pi\times800$. The integral is then

$$\frac{800^2}{(1-800^2)}\int_0^{0.01}(800\times\sin(2\pi\times\tau)-\sin(2\pi\times800\tau))d\tau=-0.25125 \tag{21}$$

For a stiff suspension $\omega_0 = 2\pi \times 10^4$ the appropriate integral is

$$\frac{0.08^2}{(1-0.08^2)}\int_0^{0.01}(0.08\times\sin(2\pi\times10^4\tau)-\sin(2\pi\times800\tau))d\tau=-8.6819\times10^{-20} \tag{22}$$

The term in brackets in Eq. (19) is ≈0 for a stiff suspension and − 0.25 for a soft suspension. This being so we may choose a stiff mount i.e., a high fundamental mode, which is more practical given the problems of vibration isolation. Mirror response can be ignored.

As mirror mounts are a major obstacle in interferometric detectors, being able to mount them in rigid platforms alleviates many problems, including noise due to Brownian motion. For all practical purposes the total excess phase is then

$$\Delta\phi_i=\sum_{i=0}^{p}\Delta\phi_i\approx p\tau_i h\frac{2\pi c}{\lambda} \tag{23}$$

We conclude from this detailed calculation that of the two independent contributions to the excess phase- time and space components - almost the entire contribution stems from the time component. The trajectory of the mirrors, whether along geodesics for free mirrors, or constrained for rigid mirrors, contributes a negligible amount to the overall phase. The excess phase is almost entirely due to the non-Euclidian geometry of the gravity wave surface.

Shot noise

The interferometer has input and output ports. The laser power at these ports is P_{in} and P_{out} respectively. The minimum sensitivity depends, among other factors, on fluctuations of the average photon number. The average photon flux is:

$$\bar{n}=\frac{P_{out}}{h\frac{2\pi c}{\lambda}}=\frac{P_{out}}{2\pi h}\frac{\lambda}{c}\sec^{-1} \tag{24}$$

The fluctuations in the average number of photons $N=\bar{n}\,\tau$ is:

$$\frac{\sigma\bar{N}}{\bar{N}}=\frac{1}{\sqrt{\bar{N}\tau_i}}$$

Under operating conditions where the mean power at the output port of the interferometer averaged over one circuit time interval is half the mean power at the input port, i.e.,

$$P_{out}=\frac{1}{2}P_{in} \tag{25}$$

also:

$$\frac{dp_{out}}{d\tau}|_{\max}=\frac{dp_{out}}{dL}|_{\max}=\frac{dL}{d\tau}=\frac{2\pi c}{\lambda}P_{in}$$

each round-trip acquires a time uncertainty of:

$$\sigma_{\delta\tau}^{i}=\frac{\sigma\bar{N}}{\bar{N}}/\frac{1}{P_{out}}\frac{dp_{out}}{d\tau}|_{\max}=\frac{1}{\sqrt{\bar{n}\tau_i}}\frac{\lambda}{2\pi c}=\pm\sqrt{\frac{h\lambda}{P_{in}\,4\pi c\tau_i}}$$

For p independent round-trips time uncertainties add in quadrature:

$$\sigma_{\delta\tau}=\pm\sqrt{\frac{h\lambda}{P_{in}\,4\pi c\tau_i}}\sqrt{\frac{1}{P}} \tag{26}$$

For a shot-noise limited detector the sensitivity is obtained by requiring the uncertainty in the shot noise to be less than the excess time delay Eq. (16):

$$\sigma_{\delta\tau}=\pm\sqrt{\frac{h\lambda}{P_{in}\,4\pi c\tau_i}}\le p\tau_i h$$

The equivalent minimum detectable metric perturbation for a laser with wavelength λ is:

$$h\ge\sqrt{\frac{h\lambda}{P_{in}\,4\pi c}}\sqrt{\frac{1}{p\tau_i}}\frac{1}{p\tau_i}$$

This expression assumes that shot noise is dominant; Brownian noise and radiation pressure noise are negligible; generally true for the example under consideration.

Detection scheme

Over-sampled detector

The expected signal is a pulse of duration τ ~ 10ms of h ~ 10^{-21} centered at a frequency of ~ 800Hz.

We can choose a sampling frequency. Generally, the minimum sampling frequency, called the Nyquist frequency, is twice the bandwidth of the signal to be sampled. For example, a signal with a bandwidth of 100Hz need be sampled every 200Hz, under ideal conditions, to be reproduced flawlessly. Practical considerations dictate the technique of ”over-sampling”, that is, sampling at rates which are integer multiples of the Nyquist frequency. The original signal is reproduced from sampled segments. Sampling permits extraction of signals even when the light spends one or more gravitational wave periods in the interferometer.

Light from a laser enters a Michelson interferometer. It passes through a beam-splitter, reflects off two mirrors onto a photodiode where the interference intensity is recorded (Figure 5); the beam exits the interferometer. The averaged intensity is that of the i-th sample. The photodiode output is averaged over an interval τ_i. Each sample is independent. τ_i is the round-trip travel time for the i-th beam.

The over-sampling frequency is f_S ~ GHz for the example we will describe, compared with the signal bandwidth f_B = 800Hz. Thus the over-sampling frequency is 10^6 times the Nyquist frequency.

We give an example of what can be achieved in an L_i = 10cm Michelson interferometer. Using a 1 watt light source of wavelength 0.545μm, and sampling every $\tau_i = (2L_i/c) = (2/3) \times 10^{-9}$secs.

Since the duration of the pulse is expected to be 10^{-2}secs, the product $p\tau_i = 10^{-2}$secs. One may collect as many as 1.5×10^7 discrete samples if we choose to integrate over the entire length of the pulse. The sensitivity is:

Copyright: ©2026 Karim et al.

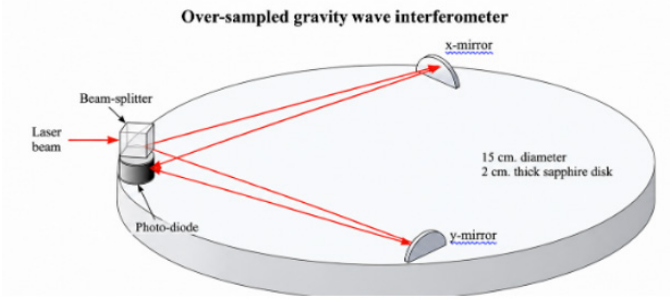

Figure 5 Schematic arrangement of interferometer components. Coherent beams reflect off the *x* — and *y* — mirrors; when they strike the photodiode they exit the interferometer. Output is sampled in discrete intervals: the intensity pattern is reconstructed using sampling algorithms. Each sample is independent, there is no multiple reflection.

$$h \geq \sqrt{\frac{h\lambda}{P_{in}\, 4\pi c}}\sqrt{\frac{1}{p\tau_i}\frac{1}{p\tau_i}}\,;\ \omega \neq \omega_0 \tag{27}$$

$$h \geq 10^{-22} \tag{28}$$

a result which depends only on the pulse duration but is noticeably independent of the sampling interval τ_i, and necessarily, the length L_i. This is also the result expected, since it confirms that the excess phase at the end of one long circuit is equivalent to the phase accumulated in many smaller circuits. The sensitivity is determined by the non-Euclidian geometry of the gravity wave surface alone.

The equivalent length of the interferometer is *1500km*, half the distance a light beam travels during the 10m*sec* gravitational wave pulse; this is also the optimum length. The sensitivity is sufficient to detect putative events from distances up to the Virgo cluster.

Unlike a Fabry-Perot cavity or a Herriot delay line where the light beam is recorded after it undergoes multiple reflections in a cavity, we note that the light beam is averaged, and recorded at the end of each round-trip. The sampled data stream is processed in accordance with algorithms used for over-sampled detection. The proposed design differs in this aspect from folded interferometers.

Proposed design

Once we realize that the sensitivity is independent of *L*, the interferometer arms are chosen for convenience to be *10cm* long; the design options also allow some flexibility. For one; a small interferometer is easier to build, easier to control the environment (temperature, pressure, isolation from external noise etc.). The entire interferometer can be mounted on single platform. Sampling the signal at the end of every round-trip prevents the accumulation of excess phase by using the beams only once.

Mechanical stability is facilitated by mounting all the components on a *15cm* diameter, *2cm* thick sapphire disk. Sapphire is a suitable material because of its low thermal expansion coefficient ($\alpha \sim 10^{-6}$/C°), excellent thermal conductivity (0.4watts/cmK°), low mechanical dissipation ($Q \approx 10^9$, reduces Brownian noise), stiff Young's modulus (~GPa) and a high speed of sound (10^4m/s),[13] so a high fundamental vibration frequency which facilitates isolation from external vibrations.

Noise from Brownian motion and radiation pressure

We can estimate the Brownian noise contribution. We use the fluctuation-dissipation theorem. The mirrors, which need be no more than *5mm* in diameter, in order to maintain a high fundamental frequency, may be sculpted directly into the sapphire disk. The entire platform vibrates due to thermal excitation.

The power spectrum of the fluctuation force is

$$F_{th}^2 = 4k_B T\,\mathrm{Re}(Z) \tag{29}$$

in terms of the impedance *Z*. The appropriate equation of motion of the mirror is

$$m\frac{\partial^2\xi}{\partial t^2} + b\frac{\partial\xi}{\partial t^2} + k\xi = F_{ext} \tag{30}$$

Or in terms of instantaneous velocity $v = i\omega\xi$:

$$i\omega m\upsilon + b\upsilon - \frac{ik\upsilon}{\omega} \equiv Z\upsilon = F_{ext}\ ;\ \therefore Z\upsilon = i\omega m + b - \frac{ik\upsilon}{\omega} \tag{31}$$

Squaring and substituting into Eq.(29) we get

$$\xi_{th}^2 = \frac{4k_B T}{\omega^2}\mathrm{Re}\left(\frac{1}{Z}\right)\frac{4k_B T}{\omega^2}\frac{b}{b^2 + (m\omega - \frac{k}{\omega})^2} \tag{32}$$

Equating $b = \omega_0 m/Q$ and $k = m\omega_0^2$, the simplified expression becomes

$$\xi_{th}^2 = \frac{4k_B T}{\omega^2}\frac{\omega_0}{mQ}\frac{1}{\left(\frac{\omega_0}{Q}\right)^2 + \left(\omega - \frac{\omega_0^2}{\omega}\right)^2} \approx \frac{4k_B T}{\omega^2}\frac{\omega_0}{mQ}\frac{\omega^2}{\omega_0^4} \tag{33}$$

for the chosen values of Q and $\omega \ll \omega_0$. Thus far below the fundamental resonance ($\omega \ll \omega_0$) the mirror amplitude excursion is:

$$\xi_{rms}^B = \sqrt{\frac{4k_B T}{Qm\omega_0^3}} = \pm 8.17\times10^{-20}\, m/\sqrt{Hz} \tag{34}$$

for T = 300K, Q ~ 10^6, m = 1kg, $\omega_0 \approx 2\pi \times 10^4$. After p discrete samples each of interval τ_i, the average excursion is

$$\xi_{rms}^B = \sqrt{\frac{4k_B T}{Qm\omega_0^3}}\sqrt{\frac{1}{\tau_i p}} = \sqrt{\frac{4k_B TQ^{-1}}{\omega m\omega_0^2}}\sqrt{\frac{c}{2L_i}}\sqrt{\frac{2L_i}{10^{-2}c}} = \pm 8.17\times10^{-20} m \tag{35}$$

ξ_{rms}^B depends on the total sampling interval, independent of the number of samples or the individual sampling interval.

The time-jitter due to Brownian motion is $\pm\,\xi_{rms}^B$ /c:

$$\xi_{rms}^B / c = \pm 2.72\times10^{-28}\,\mathrm{secs}$$

For the example under consideration the shot noise time-jitter is Eq. (26)

$$\sigma_{\delta\tau} = \pm\sqrt{\frac{h\lambda}{P_{in}\, 4\pi c\tau_i}}\sqrt{\frac{1}{P}} = \pm 10^{-24}\,\mathrm{secs}$$

The detector sensitivity Eq. (28) is limited by shot-noise in the range of frequencies $10^{-4}Hz < \omega/2\pi < 10^4 Hz$.The upper frequency limit is set by the fundamental mode of the platform and the lower limit by tidal frequencies.

Radiation pressure will also inject random vibrations in the mirrors. The fluctuating power spectrum in this case is

$$F_R^2 = 2\pi h\frac{c}{\lambda}\frac{P_{in}}{c^2} = 2\pi h\frac{c}{\lambda}\mathrm{Re}(Z) \tag{36}$$

The amplitude excursion, for *p* discrete samples each of duration τ_i, appropriate for $\omega \ll \omega_0$ is:

$$\xi^{B}_{rms} = \sqrt{\frac{2\pi hc}{\lambda m Q \omega^{3}_{0}}}\sqrt{\frac{1}{\tau_{i}}}\sqrt{\frac{1}{p}} = \pm 3.9\times 10^{-19} m \qquad (37)$$

The time uncertainty is:

$$\xi^{B}_{rms} / c = \pm 10^{-27}\,\text{secs}$$

Again this is negligible compared with the time uncertainty due to shot noise. Noise from Brownian motion and radiation pressure can be ignored.

It is worth repeating that the light beams reflect off each mirror only once, then they strike the photo-diode and are removed from the interferometer. Light from single reflections is corrupted by fluctuations in the mirror position due to radiation pressure and/or shot noise. Because each reflection is independent, the noise contributions are also independent. They add in quadrature. By contrast the situation in folded interferometers which utilize multiple reflections, is different because mirror noise fluctuations accumulate with each reflection, in practice limiting the number of folded beams.[14]

Measurement method

The photodiode detects interference fringes, actually a circular region which may be all shades from completely dark to completely bright. The photodiode output is sampled every nanosecond. To make data handling manageable, the photodiode output is fed first into an analogue integrator with a time constant which is a small fraction of the expected (reciprocal) signal frequency. For example a $10\mu sec$ time constant is sufficient for 125 samples of an *800Hz* signal or 1000 samples of a *100Hz* signal. Following the integrator the averaged signal is sent to a 16-bit analogue to digital converter and from there onto a library for comparison against different signal templates.

Referring to the earlier mention of a mode of operation Eq. (25), it turns out that re finements are needed to operate the interferometer as a null detector. Pockels cells or air columns, need to be inserted to provide phase modulation. The interferometer operation point is moved to a dark fringe.[4] Because of the stiff mounting of the mirrors, it may be possible to maintain the dark fringe condition by further slow modulation of the Pockels cells or the pressure in the air columns.

The small size of the interferometer (diameter 15cm.) facilitates operation in a vacuum environment (10^{-7}T is sufficient for $h \approx 10^{-22}$); it also opens up several schemes to isolate it from seismic vibrations which is a major source of noise at low frequencies. Isolation from ground vibrations is made easier because the design fundamental mode is $\omega_0 = 2\pi\times 10^4$ as is reduction in Brownian noise. This is one great advantage in using rigidly mounted mirrors and a high-Q platform.

The interferometer needs a laser source stabilized against both intensity and frequency drifts. Use of sapphire also minimizes platform distortions due to temperature in homogeneities. Instruments will be needed to monitor and control the temperature.

The scheme described here can be extended to a three-axis detector, which may be replicated and installed as an antenna array on several optimal locations on Earth. An array opens up the possibility of correlation interferometry which is a means to study the quantum properties of gravitational radiation.[15]

Conclusion

Working with the non-Euclidian geometry of incoming gravity waves and, using signal processing techniques we have designed a table-top 10cm Michelson interferometer with sufficient sensitivity to detect gravitational waves from in falling binary neutron stars from as far as the Virgo cluster.

Acknowledgments

We acknowledge with gratitude an anonymous referee for planting the seed of an idea, and M. Bocko for technical advice.

Conflicts of interest

The author declares that there are no conflicts of interest.

Funding

None.

References

1. Weber J. *General Relativity and Gravitational Waves*. Interscience Publishers; 1961.
2. Moss GE, Miller LR, Forward RL. Photon-noise-limited laser interferometric gravitational-wave detection. *Appl Opt*. 1971;10:2495-2498.
3. Forward RL. General relativity and the detection of gravitational radiation. *Phys Rev D*. 1978;17:379-390.
4. Weiss R. Electromagnetically coupled broadband gravitational antenna. *MIT Quarterly Progress Report*. 1972;105:54.
5. Abbott BP, Abbott R, Abbott TD, et al. LIGO Scientific Collaboration and Virgo Collaboration. Observation of gravitational waves from a binary black hole merger. *Phys Rev Lett*. 2016;116(6):061102
6. Christodoulou D. Nonlinear nature of gravitation and gravitational-wave memory. *Phys Rev Lett*. 1991;67(12):1486-1489.
7. Misner CW, Thorne KS, Wheeler JA. *Gravitation*. WH Freeman; 1973:63.
8. Hay HJ, Schiffer JP, Egelstaff PA. Measurement of the gravitational red shift in the Mossbauer effect. *Phys Rev Lett*. 1960;4:165-166.
9. Kündig W. Time dilation and the transverse Doppler effect in a rotating system. *Phys Rev*. 1963;129:2371-2375.
10. Champeney DC, Isaak GR, Khan AM. A time dilation experiment based on the Mössbauer effect. *Phys Lett*. 1963;7:241-242.
11. Isaak GR. Experimental tests of special and general relativity. *Phys Bull*. 1970;21:255.
12. Martin JL. *General Relativity*. Prentice Hall; 1988. Reprinted 1996.
13. Thorne KS. In: Hawking S, Israel W, eds. *300 Years of Gravitation*. Cambridge University Press; 1987.
14. Saphikon. *Saphikon sapphire products and materials*. 2026.
15. Saulson PR. *Fundamentals of Interferometric Gravitational Wave Detectors*. World Scientific; 1994.